Partial FFT Demodulation for Coherent Detection of OFDM Signals over Underwater Acoustic Channels

Yashar M. Aval
Northeastern University
Email: aval.y@husky.neu.edu

Milica Stojanovic
Northeastern University
Email: militsa@ece.neu.edu

***Abstract*—We propose an algorithm for coherent detection of OFDM signals over underwater acoustic channels in the presence of Doppler distortions. The algorithm uses multiple FFT demodulators, each operating on a different (partial) segment of the incoming OFDM block. The segments corresponding to several adjacent carriers and multiple receiving elements are adaptively combined to reduce the inter-carrier interference. The combiner weights are computed recursively across carriers, using a stochastic gradient algorithm. The information contained in the combiner weights is also used to predict the Doppler shifts for the next incoming block, thus enhancing the accuracy of adaptive channel tracking. Synthetic and experimental data from a recent experiment conducted over a mobile acoustic channel in the $10-15$ kHz band, show that partial FFT demodulation with enhanced channel tracking provides a significant gain in performance over a conventional coherent detector, and increases the bandwidth efficiency.**

I. Introduction

Demand for high transmission rates motivates the use of orthogonal frequency division multiplexing (OFDM) for underwater acoustic (UWA) communications as it offers robustness against the frequency-selective multipath distortion of the channel, as well as simplicity of implementation based on FFT modulation/demodulation. Detection of OFDM signals, however, is challenging in UWA channels due to the typically severe Doppler distortion which causes inter-carrier interference (ICI).

A number of techniques for ICI mitigation in UWA acoustic channels have been investigated over the past years, e.g. [1]–[5]. In [1] the authors propose ICI equalization that operates recursively across the OFDM carriers, while [2] considers sparse channel estimation methods for improved ICI equalization. Unlike these techniques that operate on a single post-FFT signal, [3] considers pre-processing based on optimal, multiple resampling of the received signal. Yet another approach is considered in [4], where multiple FFT demodulators are used to approximate the optimal receiver front-end for arbitrarily time-varying channels. This approach, termed partial FFT demodulation (P-FFT), has also been used in conjunction with differentially coherent detection in [5].

Here, we extend the receiver designed in [5] to coherent detection and introduce an enhanced channel tracking method which aids in the process of adaptive combining. The method is based on sparse channel estimation with adaptive thresholding [6], and includes a technique for predicting the Doppler shift from the combiner weights.

Performance of the algorithm is demonstrated using synthetic and experimental data obtained during the 2010 Mobile Acoustic Communications Experiment (MACE'10). Results show that P-FFT demodulation technique significantly improves the performance as compared to conventional coherent detection.

The paper is organized as follows. We describe the system model in Sec. II. The receiver algorithm is presented in Sec.III and its performance is analyzed through simulation in Sec. IV. Sec.V contains the performance results and Sec.VI summarizes the conclusions.

II. System Model

The transmitted OFDM block with K carriers is given by

$$s(t) = Re\left\{\sum_{k=0}^{K-1} d_k \mathrm{e}^{j2\pi f_k t}\right\}, t \in [0, T] \tag{1}$$

where $T = 1/\Delta f$ is the block duration and d_k is the data symbol transmitted on the k-th carrier of frequency $f_k = f_0 + k\Delta f$. Consecutive blocks are separated by a guard interval of duration T_g, which is filled with cyclic prefix or zero-padded. The rate at which the symbols are transmitted is thus $R = K/(T+Tg) = K/T'$, and the bandwidth efficiency is defined as R/B where $B = k\Delta f$.

After frame synchronization, initial resampling, downshifting by the lowest carrier frequency and cyclic prefix removal or overlap-adding [7], the signal received on the m-th element is modeled as

$$v_m(t) = \sum_k H_k^m(t) d_k e^{j2\pi k\Delta f t} + w_m(t), t \in [0, T] \tag{2}$$

where $H_k^m(t)$ represents the time-varying channel coefficient and $w_m(t)$ is the noise, assumed to be independent across the receiver array.

The signal $v_m(t)$ is first subject to P-FFT demodulation, whereby the i-th demodulator produces a partial output

$$y_{k,i}^m = \int_{iT/I}^{(i+1)T/I} v_m(t) e^{-j2\pi k\Delta f t} dt,\ i = 0, \ldots I-1 \tag{3}$$

The I outputs corresponding to the k-th carrier are now combined into a vector $\tilde{\mathbf{y}}_k^m = [y_{k,0}^m \ldots y_{k,I-1}^m]^T$, and several such vectors corresponding to adjacent carriers are grouped to form $\mathbf{y}_k^m = [\ldots \tilde{\mathbf{y}}_{k-1}^{mT}\ \tilde{\mathbf{y}}_k^{mT}\ \tilde{\mathbf{y}}_{k+1}^{mT}\ \ldots]^T$. The elements of the vector $\mathbf{y}_k^m$, of which there are L, are subject to weighted combining, which yields a variable

$$x_k^m = \mathbf{a}_k^{mH} \mathbf{y}_k^m \tag{4}$$

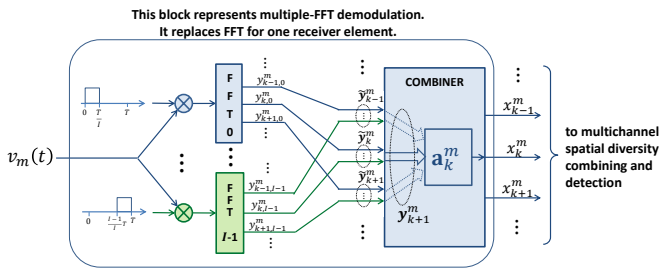

Fig. 1. Block diagram of P-FFT demodulator for one receiver element. The combiner learns weight vector $\mathbf{a}_k^m$ adaptively in carrier-by-carrier fashion.

where $\mathbf{a}_k^m$ represents the combiner weight vector and $(\cdot)^H$ denotes the Hermitian (conjugate transpose) of a matrix. The block diagram of the P-FFT demodulator is shown in Fig. 1.

The goal of combining is to compensate for the ICI, in such a manner that its output conforms to the model

$$x_k^m = H_k^m e^{j2\pi\theta_k^m} d_k + z_k^m \tag{5}$$

where H_k^m is a complex-valued channel coefficient, θ_k^m accounts for phase shift caused the Doppler frequency offset, and z_k^m contains the noise. More precisely, if we label the consecutive OFDM blocks by $n = 0, 1, \ldots$, they will be associated with the channel coefficients $H_k^m(n)$ and the phases $\theta_k^m(n)$. While we make no assumptions about the channel coefficients other than that they are varying slowly from one block to another, we model the phases as

$$\theta_k^m(n+1) = \theta_k^m(n) + 2\pi f_k a_m(n) T' \tag{6}$$

where $a_m(n)$ represents the dominant Doppler scaling factor corresponding to the m-th receiving element during the n-th block. We will refer to this model later when we discuss phase prediction.

Given the combiner outputs $x_k^1, \ \ldots, \ x_k^M$ corresponding to the multiple receiving elements, an estimate of the data symbol d_k is formed as

$$\hat{d}_k = \frac{\sum_m H_k^{m*} x_k^m}{\sum_m |H_k^m|^2} \tag{7}$$

The above operation reflects maximum ratio combining (MRC) of M spatially distinct elements of the receiver array.

III. Receiver Algorithm

The receiver algorithm is summarized in Fig. 2. The algorithm begins with the first block ($n = 0$) within a frame of OFDM blocks. For this block, the combiner weights are set to all-ones vectors, $\mathbf{a}_k^m = \mathbf{1}$, which are used to form the variables x_k^m. The channel coefficients H_k^m are then estimated using pilot symbols and the thresholding algorithm [6] which exploits the channel sparseness in the impulse response domain by setting the sparsing threshold just above the noise level. We denote these channel estimates by $\hat{H}_k^m(0)$. The initial phases and the estimates of the Doppler factors a_m are set to zero, $\hat{a}_m = 0$, resulting in the phase predictions $\hat{\theta}_k^m(1) = 0$.

The algorithm now proceeds in each new block ($n = 1, 2, \ldots$) as follows. Using the existing channel

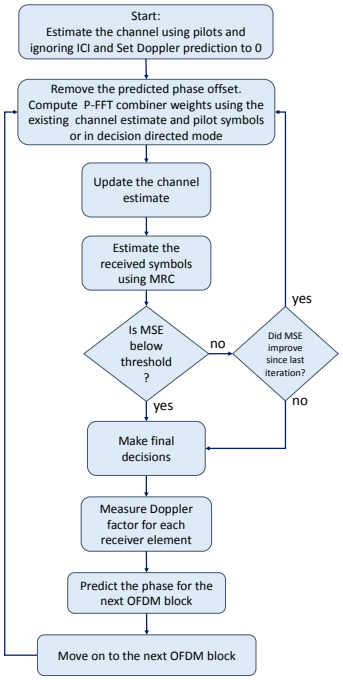

Fig. 2. Block diagram of the receiver algorithm.

estimates from the previous block $\hat{H}_k^m(n-1)$, the phase predictions $\hat{\theta}_k^m(n)$, and the available pilot symbols, it first computes the combiner weights. This computation is carried out recursively across carriers, beginning with the lowest carrier with an initial weight vector a_0^m taken from the previous block and using a stochastic gradient algorithm.[1] Specifically, the combiner weights are computed as[2]

$$\mathbf{a}_{k+1}^m = \mathbf{a}_k^m + \mu \mathbf{y}_k^m e_k^{m*}, \ k = 0, 1, \ldots \tag{8}$$

where

$$e_k^m = \hat{H}_k^m(n-1) d_k - x_k^m e^{-j\hat{\theta}_k^m(n)} \tag{9}$$

is the driving error obtained using $x_k^m = \mathbf{a}_k^{mH} \mathbf{y}_k^m$, and μ is an a-priori chosen step-size. This process is performed for all receiving elements, $m = 1, \ldots M$.

The data symbols corresponding to the first K_p carriers are the known pilot symbols (except in the first block, where all the carriers serve as pilots). These pilot symbols are used as the training sequence for the adaptive algorithm. The data symbols are then estimated according to (7) and the symbol decisions made on the so-obtained estimates are used to continue the recursive computation of combiner weights over the remaining carriers.

Once the combiner weights have been updated, the signals x_k^m are used to form the new channel estimates $\hat{H}_k^m(n)$. Channel estimation is performed as before, using the adaptive thresholding algorithm [6]. The so-obtained channel estimates will be passed on to the next block.

[1] A different algorithm can be used as well, e.g. the recursive least squares algorithm, but it suffices to focus on the simple least mean squares algorithm to illustrate the approach.

[2] We drop the obvious index n on the weight vectors $\mathbf{a}_k^m$, the signals $\mathbf{y}_k^m$ and x_k^m, and the errors e_k^m.

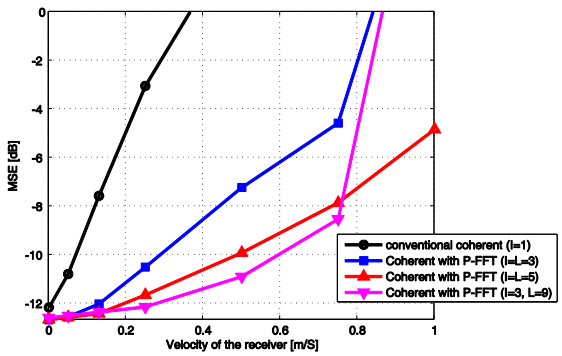

Fig. 3. Average MSE performance of coherent detection with and without P-FFT demodulation vs. speed of transmitter motion, based on simulation using Full-VirTEX [8]. The nominal geometry is that of the MACE'10 experiment, shown in Fig. 4. The average SNR at the input to each of the $M = 4$ receiving elements is 10 dB.

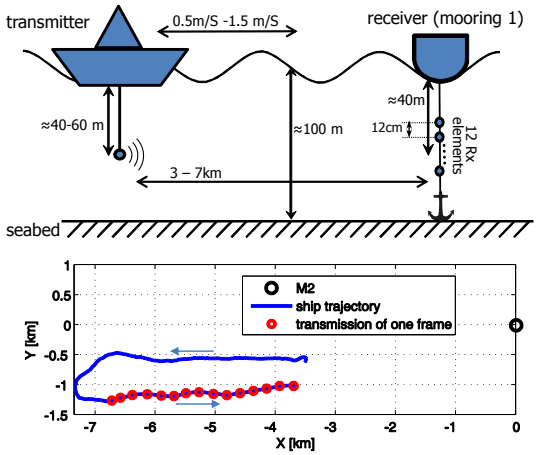

Fig. 4. Top: Nominal geometry of the MACE'10 experiment. Bottom: trajectory of the transmitter. Receiver location is indicated by the large circle on the right. The transmitter first moves away from the receiver, then towards the receiver, at velocity up to 1.5 m/s. We analyze the performance based on 15 transmission made when the transmitter moves towards the receiver (small circles), which span approximately 1 hour. Each transmission consists of 6 frames of OFDM blocks, with each frame containing 2^{13} QPSK symbols. Each frame uses a different number of OFDM carriers, ranging from 2^6 to 2^{11} carriers.

An additional step can also be included at this point, whereby the overall mean squared error (MSE) in data detection, $\sum_k |d_k - \hat{d}_k|^2$, is monitored, and if found unsatisfactory, the procedure is repeated. In this manner, the estimates are refined iteratively, until a satisfactory MSE level is achieved (or the procedure aborted).

As the last step, the Doppler factors are estimated and the phase predictions are made for the next block. The Doppler factors are estimated by measuring the phase change across the elements of the combiner weight vector $\mathbf{a}_k^m$. This phase change can be estimated simply as the end-point difference $\Delta\alpha_k^m = \angle a_{k,I-1}^m a_{k,0}^{m\,*}$, or from a linear fit between the phases of all the elements of $\mathbf{a}_k^m$. Given $\Delta\alpha_k^m$, the Doppler scaling factor is estimated as

$$\hat{a}_m(n) = \frac{1}{K(\frac{I-1}{I})T} \sum_{k=0}^{K-1} \frac{\Delta\alpha_k^m}{2\pi f_k} \tag{10}$$

The predictions on the phases θ_k^m are now made as

$$\hat{\theta}_k^m(n+1) = \hat{\theta}_k^m(n) + 2\pi\hat{a}_m(n) f_k T' \tag{11}$$

The algorithm now moves on to the next block.

IV. Simulation Results

In this section, we assess the average performance of the proposed receiver algorithm through simulation. We use Full-VirTEX [8] to simulate the time-varying UWA channel.

The simulation geometry is similar to that of the MACE'10 experiment. Specifically, we use the recorded sound speed profile, trasmitter/receiver depth and receiver array structure of Fig. 4. We choose the wave height to be 2 m peak-to-peak and the receiver to be approximately 1.5 km away from the transmitter. We produce 5 geometries which differ slightly in the shape of the seabed and surface motion, analyze the performance of each method for each of the geometries, and report the average MSE. All of the simulations in this section are based on OFDM blocks with 512 carriers, transmitted over the acoustic frequency band 10.5 kHz - 15.5 kHz. The motion is considered to be at a constant speed during each frame containing 16 OFDM blocks.

Fig. 3 shows the MSE as a function of the relative transmitter/receiver velocity for coherent detection with P-FFT demodulation and compares it with that of conventional detection. Conventional detection is seen to be very sensitive to motion-induced Doppler distortion and will fail if the receiver moves any faster than 0.1 m/s in this case. P-FFT demodulation, in contrast, adds robustness against Doppler shifts, and the robustness improves with the number of partial segments I.

V. Experimental Results

In this section, we provide the experimental results from the MACE'10 trials which were conducted during the summer of 2010, about 60 miles south of Rhode Island, using the acoustic frequency range between 10.5 kHz and 15.5 kHz. Fig. 4 shows the approximate channel geometry, the structure of the receiver array, and the trajectory of the transmitter during the experiment, and Table I summarizes parameters of the signals transmitted during this experiment. The results provided in this section represent averages made over 15 transmissions repeated every four minutes, spanning 1 hour.

Figures 5 and 6 summarize the performance results obtained using P-FFT demodulation and adaptive combining. When OFDM blocks are short, ($T' = 30$ ms at $K = 64$), there is little channel variations between OFDM blocks and therefore the coherent receiver easily tracks the channel variations from one OFDM block to the next. As the number of carriers grows,

TABLE I
OFDM signal parameters used for the MACE'10 experiment

No. of carriers, K	64	128	256	512	1024	2048
No. of blocks per frame	128	64	32	16	8	4
carrier spacing Δf [Hz]	76	38	19	9.5	4.8	2.4
transmission rate [kbps]	4.4	6	7.5	8.5	9	9.4
bandwidth eff. [bit/Hz]	0.9	1.24	1.53	1.74	1.86	1.93

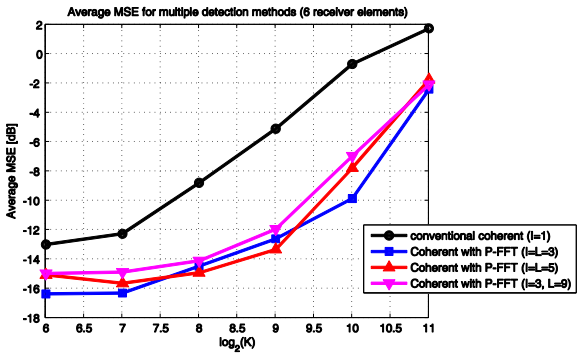

Fig. 5. Average MSE performance of coherent detection with and without P-FFT demodulation ($M = 6$ receiving elements). As the number of carriers grows, the performance of the conventional coherent receiver (single FFT) degrades significantly. P-FFT demodulation boosts the performance of the receiver by several dB and provides reliable performance even with 512 carriers.

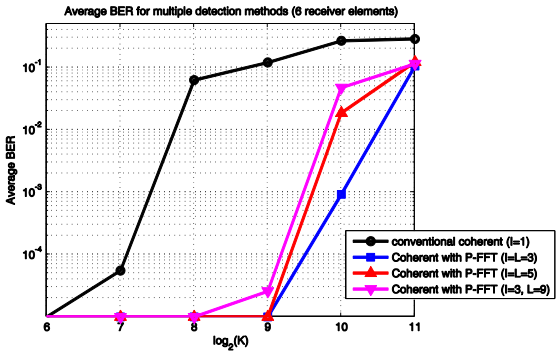

Fig. 6. Average BER performance of coherent detection with and without P-FFT demodulation, ($M = 6$ receiving elements). The input signal-to-noise ratio is estimated to be on the order of 20 dB. No error correction coding is employed.

ICI degrades the performance of the conventional receiver significantly. This is where P-FFT enhances the performance. It notably does so by reducing the ICI and improving the channel tracking accuracy to arrive at an outstanding performance (no errors observed during transmission of $250,000$ bits without the use of error correction coding) even as we pack 512 carriers into 5 kHz of bandwidth (resulting in the narrow carrier spacing of 9.5 Hz). If the number of carriers is increased further, all detection methods eventually fail with 2048 carriers due to sever Doppler shifts and reduced coherence between adjacent OFDM blocks will result in occasional loss of channel tracking.

Comparing the performance among various receiver structures characterized by different (I, L) choices, we note that a relatively small receiver size with $I = 3$ and $L = I = 3$ suffices to improve the performance. Increasing either the number of partial segments I while keeping $L = I$ (effectively using a single-tap ICI equalizer), or increasing the equalizer span while keeping I fixed ($L = 3I$ effectively corresponds to a three-tap ICI equalizer), does not result in additional improvement in the present data set. The MACE'10 data is primarily characterized by fast motion, as well as variable surface conditions. These observations support our implicit conjecture that OFDM signal detection on highly Doppler-distorted channels benefits from front-end filtering. Partial FFT demodulation implements adaptive front-end filtering in a computationally-efficient manner, and demonstrates the ability to deal with the Doppler distortion even without additional ICI equalization.

VI. Conclusions

We proposed a coherent receiver based on partial FFT demodulation for detection of OFDM signals over UWA channels with severe Doppler distortion where random, time-varying frequency shifts can be comparable with the carrier spacing. The proposed receiver replaces the conventional, single FFT demodulator with a few (e.g. three) FFTs whose outputs are combined in a manner that minimizes post-detection error. The receiver also incorporates spatial diversity combining, an adaptive sparse channel estimator and a phase prediction method to track the channel response across OFDM blocks.

Synthetic and experimental data were used to demonstrate the performance of the receiver, showing that a substantial improvement is available from partial FFT demodulation over the conventional, single-FFT demodulation (7 dB at 512 carriers within 5 kHz of bandwidth). This improvement is similar to the improvement obtained by a same-size partial FFT demodulator applied to a differentially coherent receiver. For the MACE'10 experiment, no bit errors were observed during transmission of 250,000 bits spanning 1 hour (without the use of error correction coding).

Future work on this topic will include alternative receiver algorithms, extensions to multiple FFT demodulation methods that use signal projections other than partial windowing, and inclusion of error correction coding.

Acknowledgement

This work was supported in part by the ONR grants N00014-07-1-0738 and N00014-09-1-0700, and NSF grant CNS-1212999.

References

[1] K. Tu, D. Fertonani, T. Duman, M. Stojanovic, J. Proakis, and P. Hursky, "Mitigation of intercarrier interference for OFDM over time-varying underwater acoustic channels," *IEEE J. Ocean Eng.*, vol. 36, Apr. 2011.

[2] C. R. Berger, S. Zhou, J. C. Preisig, and P. Willett, "Sparse channel estimation for multicarrier underwater acoustic communication: From subspace methods to compressed sensing," *IEEE Trans. Sig Proc.*, vol. 58, no. 3, 2010.

[3] K. Tu, T. Duman, M. Stojanovic, and J. Proakis, "Multiple-resampling receiver design for OFDM over Doppler-distorted underwater acoustic channels," *IEEE J. Ocean Eng.*, 2013.

[4] S. Yerramalli, M. Stojanovic, and U. Mitra, "Partial FFT demodulation: A detection method for highly Doppler distorted OFDM systems," *IEEE Trans on Sig. Proc.*, vol. 60, no. 11, Nov. 2012.

[5] Y. Aval and M. Stojanovic, "A method for differentially coherent multichannel processing of acoustic OFDM signals," in *7th IEEE Sensor Array and Multichann. Sig. Proc. Workshop (SAM)*, Jun. 2012.

[6] E.Valera and M.Stojanovic, "Space-frequency coded OFDM for underwater acoustic communications," in *IEEE OCEANS'12 Conf., Virginia Beach*, Oct. 2012.

[7] B. Muquet, W. Zhengdao, G. Giannakis, M. D. Courville, and P. Duhamel, "Cyclic prefixing or zero padding for wireless multicarrier transmissions?" *IEEE Trans. on Commun.*, vol. 50, no. 12, Dec. 2002.

[8] J. C. Peterson and M. B. Porter, "Virtual timeseries experiment (VirTEX) - quick start," http://oalib.hlsresearch.com/Rays/VirTEX/README.pdf, 2011, [Online; accessed March-2013].